

Molecular-Level Insight into the Interaction of Phospholipid Bilayers with Cellulose

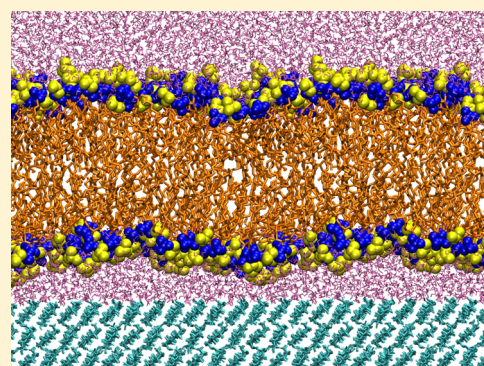
Andrei Yu. Kostritskii,[†] Dmitry A. Tolmachev,[‡] Natalia V. Lukasheva,[‡] and Andrey A. Gurtovenko^{*,‡}

[†]Faculty of Physics, St. Petersburg State University, Ulyanovskaya str. 3, Petrodvorets, St. Petersburg, 198504 Russia

[‡]Institute of Macromolecular Compounds, Russian Academy of Sciences, Bolshoi Prospekt V.O.31, St. Petersburg, 199004 Russia

Supporting Information

ABSTRACT: Molecular-level insight into the interactions of phospholipid molecules with cellulose is crucial for the development of novel cellulose-based materials for wound dressing. Here we employ the state-of-the-art computer simulations to unlock for the first time the molecular mechanisms behind such interactions. To this end, we performed a series of atomic-scale molecular dynamics simulations of phospholipid bilayers on a crystalline cellulose support at various hydration levels of the bilayer leaflets next to the cellulose surface. Our findings clearly demonstrate the existence of strong interactions between polar lipid head groups and the hydrophilic surface of a cellulose crystal. We identified two major types of interactions between phospholipid molecules and cellulose chains: (i) direct attractive interactions between lipid choline groups and oxygens of hydroxyl (hydroxymethyl) groups of cellulose and (ii) hydrogen bonding between phosphate groups of lipids and cellulose's hydroxymethyl/hydroxyl groups. When the hydration level of the interfacial bilayer/support region is low, these interactions lead to a pronounced asymmetry in the properties of the opposite bilayer leaflets. In particular, the mass density profiles of the proximal leaflets are split into two peaks and lipid head groups become more horizontally oriented with respect to the bilayer surface. Furthermore, the lateral mobility of lipids in the leaflets next to the cellulose surface is found to slow down considerably. Most of these cellulose-induced effects are likely due to hydrogen bonding between lipid phosphate groups and hydroxymethyl/hydroxyl groups of cellulose: the lipid phosphate groups are pulled toward the water/lipid interface due to the formation of hydrogen bonds. Overall, our findings shed light on the molecular details of the interactions between phospholipid bilayers and cellulose nanocrystals and can be used for identifying possible strategies for improving the properties of cellulose-based dressing materials via, e.g., chemical modification of their surface.



INTRODUCTION

Biodegradable polymers have attracted a great deal of attention over last decades in view of their high potential for numerous biomedical applications. This is in line with a general trend of replacing synthetic materials with ones coming from natural sources. One of the typical representatives of such natural biodegradable polymers is cellulose.¹ Cellulose, being the most abundant renewable organic material on Earth, is easily accessible, relatively cheap, nontoxic, and biocompatible. Cellulose is mainly extracted from plants and can also be produced by bacteria in a well-controlled biotechnological process (bacterial cellulose). Many practical applications of cellulose-based materials include tissue engineering, bone implanting, and the use as biocompatible nanocomposites with antimicrobial properties.^{2–6} Another important application of composite materials based on cellulose is wound dressing.³ Wound dressings are of tremendous importance since they are in direct contact with the wound: a dressing material interacts with tissues and inevitably with the surface of cells, i.e., with cell membranes. Despite the importance of such interactions for the overall healing process, very little is known about the molecular

picture of the interfacial region between the dressing and the cell membrane.

In this paper, we employ the state-of-the-art computer simulations to explore for a first time the interactions of the surface of a cellulose nanocrystal with model phospholipid membranes at atomistic resolution. A molecular-level insight into such interactions is beyond the resolution of most experimental techniques and can be extremely useful for identifying the factors that are crucial for improving the properties of cellulose-based dressing materials through, e.g., chemical modification of their surface. To the best of our knowledge, phospholipid bilayers on a solid support made of crystalline cellulose have never been studied with the use of computer simulations.

As such, our computational study falls into the category of computer simulations of supported lipid bilayers with a cellulose crystal as a support. Although conventional free-standing lipid bilayers have extensively been studied through

Received: July 3, 2017

Revised: October 3, 2017

Published: October 17, 2017

computer simulations over last two decades, the computational studies of supported lipid bilayers are still relatively rare. Atomic-scale computer modeling was employed to get insight into the structural and dynamical properties of phospholipid bilayers on supports made of hydroxylated amorphous silica⁷ and α -quartz⁸ as well as on nanoporous substrates of various degree of hydrophilicity.^{9,10} In addition to atomistic simulations, there are a number of studies in which computational models of lower resolution (coarse-grained models) were used.^{11–14} Both atomistic and coarse-grained studies of supported lipid bilayers revealed the existence of support-induced asymmetry in the structure and dynamics of the opposite bilayer leaflets. An impact of a solid support on lipid membranes apparently depends on the properties of the support (such as e.g. its hydrophobicity or hydrophilicity).

Overall, one can distinguish two types of supported lipid bilayer systems studied by far through computer simulations. These are lipid bilayers on a solid support^{7,8} and bilayers on a nanoscopically structured (porated) support (so-called semi-supported bilayers).^{9,10} The latter allow the bulk water to get access to the interfacial region between the bilayer and the support. In the case of a cellulose crystal (fibril), the support surface has no pores, so that the information regarding the proper hydration of the interfacial region is not easily accessible. To this end, here we focus on the structural and dynamic properties of cellulose-supported phospholipid bilayers at various levels of the interfacial hydration (and correspondingly, at various distances between the bilayer and the cellulose support). Essentially, our findings reveal strong interactions of hydroxymethyl and hydroxyl groups of the cellulose surface with the polar lipid head groups. These interactions, being increasingly important upon reducing the interfacial hydration (or the bilayer-support distance), change drastically the properties of the lipid/water interface of a bilayer leaflet proximal to cellulose.

METHODS AND MODELS

We have performed atomic-scale molecular dynamics simulations of a palmitoyloleoylphosphatidylcholine (POPC) lipid bilayer placed in the vicinity of the surface of crystalline bacterial cellulose; see Figure 1. The bilayer–cellulose distance was systematically varied through the change in the hydration level of lipid head groups of the bilayer leaflet proximal to the cellulose-based support. Overall, we considered 4 lipid–cellulose systems with the numbers of water molecules per lipid being in the range from 30 (full hydration) to 0 (“dry” interface); see Table 1.

A crystalline structure of bacterial cellulose was built up according to the procedure outlined in detail in our previous papers.^{15,16} It is largely based on crystallographic data¹⁷ for the cellulose I β and consists of three layers of cellulose chains. A single crystal layer contains 12 cellulose chains with 6 cellobiose units each; see Figure 2. The periodic boundary conditions are applied in all three directions. To simulate an infinite crystal surface, the cellulose chains were covalently linked to their periodic images. This imposed a condition of a fixed (“incompressible”) surface area for a lipid bilayer that is placed on the top of a cellulose crystal. In other words, the total area of a cellulose crystal patch in a simulation box (X – Y plane) dictates the size of a lipid bilayer. For the cellulose crystal considered in our study, the box size in X - and Y -directions was fixed to 6.18 and 6.5 nm, respectively, amounting to the total surface area of 40.17 nm². In turn, a POPC lipid bilayer consisted of 124 lipids (62 lipids per leaflet). The overall number of POPC lipids per leaflet was carefully adjusted in such a way that the equilibrium area per lipid (~ 0.65 nm²) of a POPC bilayer matched closely the experimental¹⁸ and computational data.¹⁹

The cellulose–bilayer systems were hydrated with water molecules; the overall number of H₂O molecules in the systems was in the range

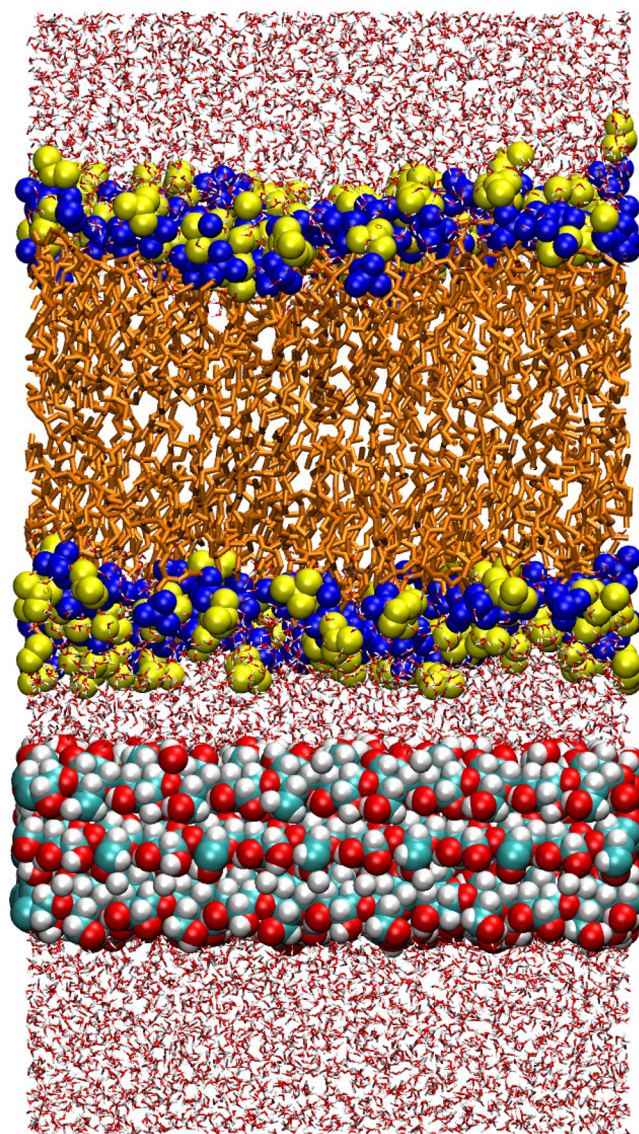


Figure 1. Snapshot of a cellulose–bilayer system (the system POPC–CEL–30H₂O is shown). Lipid head groups are shown in yellow and blue, lipid tails in orange, a cellulose crystal in red, cyan, and white, and water molecules in red.

Table 1. Simulated Lipid–Cellulose Systems

system	N_{water}^a	simulation time [ns]
POPC–CEL–30H ₂ O	30	500
POPC–CEL–20H ₂ O	20	500
POPC–CEL–10H ₂ O	10	500
POPC–CEL–0H ₂ O	0	700
POPC124 ^b		500

^aThe number of water molecules per lipid in the bilayer leaflet proximal to the cellulose surface. ^bA fully hydrated free-standing lipid bilayer.

from 5117 (POPC–CEL–0H₂O system) to 7591 (POPC–CEL–30H₂O system). As mentioned above, the number of water molecules per lipid in the proximal bilayer leaflet varied from 0 to 30. The opposite (distal) leaflet was hydrated with an excess of water (90–100 H₂O molecules per lipid), ensuring that the distal bilayer leaflet did not interact with the periodic image of a cellulose crystal (the corresponding distance was at least 4 nm). A free-standing bilayer (POPC124 system) was hydrated with 4800 H₂O molecules. The total

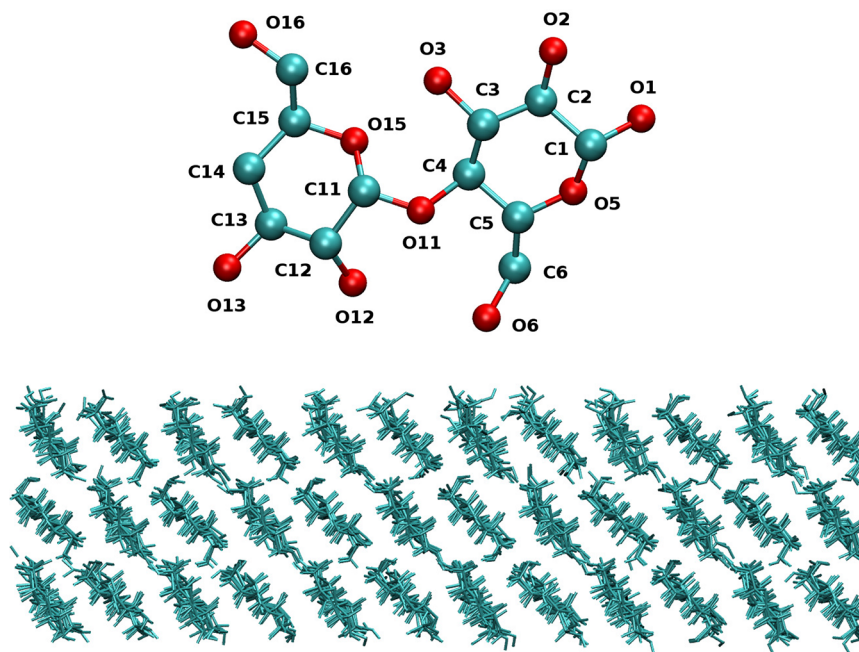


Figure 2. (Top) Chemical structure and atom numbering of a cellobiose unit. Carbon atoms are shown in cyan and oxygen atoms are shown in red. (Bottom) Side view on a three-layer cellulose crystal considered in this study.

number of atoms in the simulated systems was in the range from $\sim 41\,000$ to $\sim 48\,500$.

Cellulose monosaccharides were described in the frame of the CHARMM35 force-field.²⁰ To handle glycosidic linkages in a cellobiose unit (see Figure 2), some of the parameters were modified according to ref 21. In general, none of the existing force-fields can preserve a two-dimensional network of intermolecular hydrogen bonds which is observed in experiments for the $I\beta$ crystal structure.¹⁶ Furthermore, all the cellulose models lead to a fibril twisting.^{22,23} However, our primary goal is to get insight into the interactions of a lipid bilayer with the surface of a cellulose crystal. Therefore, we chose to consider a “frozen” inner structure of the cellulose crystal by imposing position restraints on all heavy atoms of monosaccharide rings, except exocyclic groups and hydroxyl oxygens. Lipid molecules were described through an extensively validated force-field CHARMM36;¹⁹ this force-field is fully compatible with the model used for cellulose. Water was represented by the CHARMM version of TIP3P model.²⁴

All simulations were carried out in the NAP_zT ensemble at $T = 310$ K and $P = 1$ bar. Pressure was controlled semiisotropically, and the thermostat was applied separately to a cellulose crystal, a lipid bilayer, and water molecules. Each system was initially equilibrated for 50 ns with the Berendsen scheme²⁵ used for both thermostat and barostat. For production runs (500–700 ns long, see Table 1), we switched to the Nosé–Hoover thermostat^{26,27} and the Parrinello–Rahman barostat.²⁸ All hydrogen bonds were constrained with the LINCS algorithm.²⁹ A Lennard–Jones switching function over 1–1.2 nm was used, while the particle-mesh Ewald method³⁰ with a real-space cutoff of 1.2 nm was employed to handle electrostatic interactions. The time step was 2 fs. The GROMACS software (v. 5) was used for all the simulations.³¹

To explore possible size effects, we increased the size of one of the cellulose-bilayer systems (POPC-CEL-10H₂O system) in such a way that the box length in both X - and Y -directions (the lipid bilayer plane) was doubled, leading to a system that was 4 times larger than the original one. In this cellulose–bilayer system a single crystal layer contained 24 cellulose chains with 12 cellobiose units each and a lipid bilayer consisted of 496 POPC lipids (248 lipids per leaflet). The system was hydrated with 25 300 water molecules; the total number of atoms amounted to $\sim 178\,500$. To speed up the initial equilibration, a well equilibrated configuration of the original POPC-CEL-10H₂O

system (at $t = 450$ ns) was used for building up the system of a larger size. The resulting system was pre-equilibrated for 10 ns with the Berendsen scheme; the production run (with the Nosé–Hoover thermostat and the Parrinello–Rahman barostat) was 200 ns long (last 100 ns were used for subsequent analysis). Overall, we did not find any noticeable impact of the system size on the main conclusions of our study; see the Supporting Information for details (Figures S4–S6 and Tables S1 and S2).

RESULTS AND DISCUSSION

Equilibration and Interaction Energies. Before actual calculations of structural and dynamic characteristics of cellulose-supported bilayer systems, one needs to ensure that the systems are properly equilibrated. To this end, we calculated the distance between centers of mass of a lipid bilayer and a cellulose crystal along the Z -axis (the bilayer normal) and also the minimum distance between atoms of a lipid bilayer and a cellulose crystal; see Figures S1 and S2. This gives us an estimate of the time needed for a bilayer to adjust itself nearby the cellulose surface. It is seen that the initial equilibration requires less than 100 ns for the systems with water molecules present in the bilayer–cellulose interfacial region (Figure S1) and ~ 300 ns for the “dry” POPC-CEL-10H₂O system (Figure S2).

As the interfacial water bath between the bilayer and the cellulose surface is not coupled to bulk water in the systems under study, one needs to ensure that there is no net flux of water molecules across the bilayer. Such an effect was reported by Xing and Faller¹¹ in coarse-grained MD simulations of lipid bilayers on a solid support. In Figure 3, we plot a relative change in the number of water molecules in the interfacial bilayer–cellulose region with respect to the initial water content. It is seen that transport of water molecules across a bilayer is present in all bilayer–cellulose systems. However, for the systems with a nonzero level of initial hydration (POPC-CEL-30H₂O, POPC-CEL-20H₂O, and POPC-CEL-10H₂O), water molecules diffuse across the bilayer in both directions (we note that no water molecules reside within the bilayer interior).

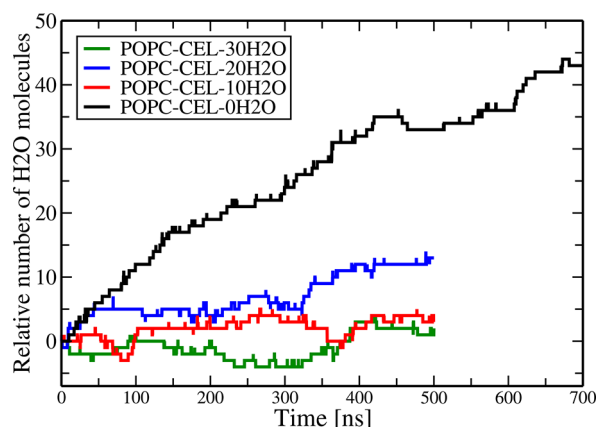


Figure 3. Relative change in the number of water molecules in the interfacial bilayer–cellulose region with respect to the initial water content.

In contrast, for the POPC-CEL-0H₂O system, we see a net flux of water molecules across the bilayer (Figure 3), leading to the appearance of water molecules in the initially “dry” interface. Overall, the diffusion of water molecules across the hydrophobic core of a lipid bilayer occurs very rapidly, while a water molecule can spend several nanoseconds in the lipid head group region before it reaches the bilayer–cellulose interface; see Figure S3 for an illustration. Note, as the overall number of leaked water molecules is relatively small (~ 40), the distance between a bilayer and a support does not seem to be influenced; see Figure S2. In general, a net water flux implies that the system is not in equilibrium yet. Xing and Faller¹¹ demonstrated that one needs around 7 μ s for the net water flux to disappear. Therefore, we can conclude that a proper equilibration of the “dry” POPC-CEL-0H₂O system requires 1 order of magnitude longer simulation times as compared to the rest of the systems, which is computationally prohibitive.

Thus, in the following we focus mostly on the properties of well-equilibrated POPC-CEL-30H₂O, POPC-CEL-20H₂O, and POPC-CEL-10H₂O systems. However, we decided to include also the POPC-CEL-0H₂O system in our calculations for illustration purpose only. This system corresponds to a limiting situation of a “dry” interface and is therefore of much interest, although one should always keep in mind that the system is not properly equilibrated.

In Table 2, we summarized the interaction energies (electrostatic and Lennard–Jones components) for proximal leaflets of POPC bilayers, cellulose layers adjusted to bilayer leaflets, and interfacial water molecules between the bilayer and

the cellulose. All the characteristics (here and in the following) were averaged over last 400 ns of MD trajectories.

First of all, one can see a very substantial contribution to the energy due to water molecules for both the bilayer and the cellulose crystal; this hydration energy stays almost the same for the systems with 30 and 20 H₂O molecules per lipid in the interfacial region, slightly decreasing for the system POPC-CEL-10H₂O. One of the most interesting contribution is the interaction energy between the lipid bilayer and cellulose. For the POPC-CEL-30H₂O system this energy is practically zero, indicating the absence of lipid–cellulose interactions in this system. For the rest of the systems it is nonzero and negative and its absolute value increases with dehydration of the interfacial region. However, to make a definitive conclusion regarding the nature of the cellulose–bilayer interactions, one needs to perform free-energy calculations. Interestingly, in the POPC-CEL-20H₂O system electrostatic and Lennard–Jones interactions contribute equally to the bilayer–cellulose interactions, while for the POPC-CEL-10H₂O system the electrostatics prevails; see Table 2. In the subsequent sections, we will discuss how the bilayer–cellulose interactions affect the structural and dynamic properties of the systems under study.

Mass Density Profiles and Water Orientation. The impact of a cellulose support on a lipid bilayer can easily be explored through evaluating the density profiles of key components of a system (lipid, water, and cellulose). In Figure 4, we present the mass density profiles for all bilayer–cellulose systems at hand (all profiles are centered with respect to the center of mass of a lipid bilayer). First of all, it is seen that the lipid density profiles for distal leaflets are very similar for all four systems and characterized by a conventional shape typical for fully hydrated free-standing phospholipid bilayers. Furthermore, the density profiles of water at the distal bilayer leaflets are not influenced by a cellulose crystal and demonstrate a behavior typical for bulk water (see Figure 4 at $z > 4$ nm). As for the leaflets next to the cellulose crystal, they remain largely unaffected by the support when the hydration level is relatively large. This is the case for the systems with 30 and 20 water molecules per lipid in the proximal leaflet, although in latter case one can see contacts of lipids with cellulose as well as a pronounced change in the density profile of the interfacial water (see Figure 4). Lower levels of hydration lead to strong interactions between lipids and the cellulose surface and correspondingly to a pronounced asymmetry in the density profiles of the opposite bilayer leaflets. In particular, for the system with low hydration (POPC-CEL-10H₂O), the density profile for the proximal leaflet is characterized by the appearance of two peaks (instead of one maximum for systems POPC-CEL-30H₂O and POPC-

Table 2. Electrostatic and Lennard–Jones Components of the Interaction Energies [kJ/mol] for Proximal Leaflets of POPC Bilayers, Proximal Layers of Cellulose Crystals and Water Molecules between the Bilayer and Cellulose

	bilayer–cellulose	bilayer–water	cellulose–water
POPC-CEL-30H ₂ O, Coulomb	1 ± 7	−21 769 ± 548	−6679 ± 241
POPC-CEL-30H ₂ O, LJ	−6 ± 6	−1888 ± 137	−863 ± 80
POPC-CEL-20H ₂ O, Coulomb	−174 ± 101	−21 912 ± 541	−6562 ± 253
POPC-CEL-20H ₂ O, LJ	−196 ± 46	−1819 ± 139	−772 ± 83
POPC-CEL-10H ₂ O, Coulomb	−1654 ± 207	−19 168 ± 483	−5395 ± 257
POPC-CEL-10H ₂ O, LJ	−984 ± 52	−1163 ± 122	−426 ± 77
POPC-CEL-0H ₂ O, Coulomb	−6433 ± 163	−2308 ± 361	−415 ± 68
POPC-CEL-0H ₂ O, LJ	−2357 ± 66	37 ± 46	−14 ± 23

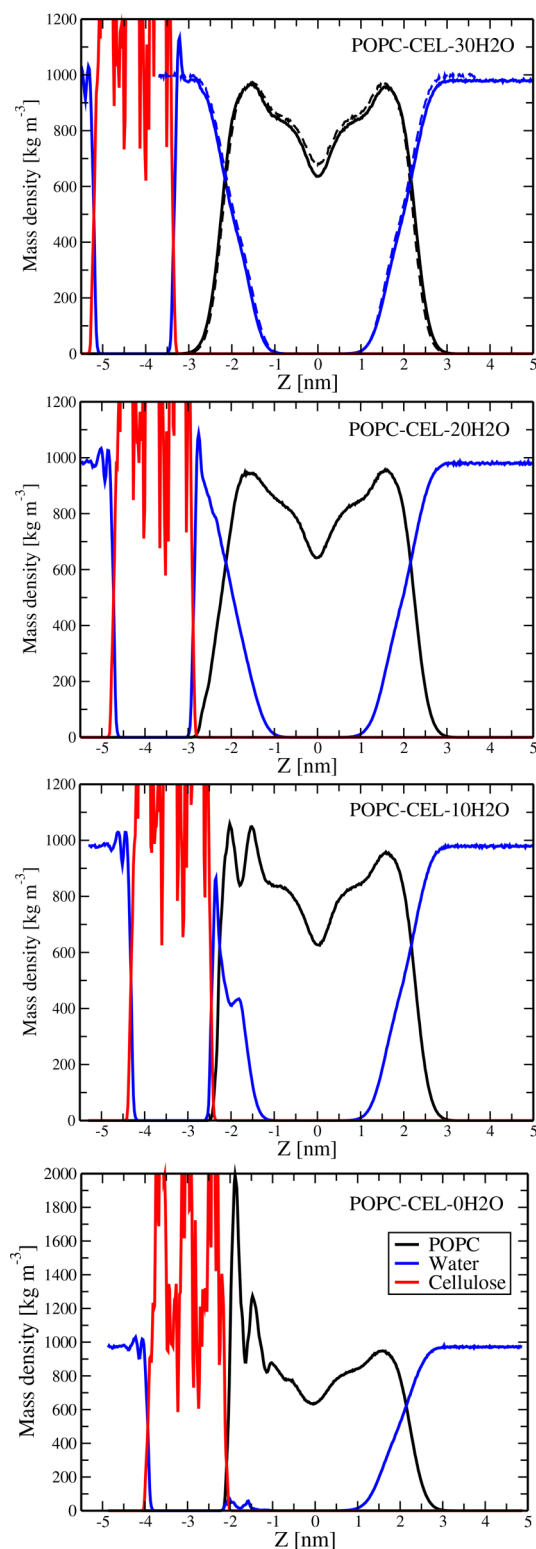


Figure 4. Mass density profiles for lipids (black), water molecules (blue) and cellulose (red) for all considered cellulose–bilayer systems as a function of the distance from the bilayer center ($Z = 0$). The profiles for a free-standing bilayer are shown by dashed lines (top plot).

CEL-20H₂O, see Figure 4). For the “dry” system (POPC-CEL-0H₂O), these effects are even more pronounced. It is also noteworthy that starting from the hydration level of 20 water molecules per lipid, the properties of the interfacial water phase

are subject to significant changes as a so-called “bulk” water does not seem to present between a bilayer and a cellulose crystal any more.

To get a more detailed insight into the influence of a cellulose support on a lipid bilayer, in Figure 5, we present the component-wise density profiles for some key atomic groups of the proximal bilayer leaflet and the cellulose layer next to the bilayer. Oxygen atoms O2(O12) and O3(O13) of hydroxyl groups as well as oxygen atoms O6(O16) of exocyclic hydroxymethyl groups (groups of carbon C6(C16)) are shown for cellulose chains; see Figure 2 for the numbering of cellulose atoms. In turn, nitrogen atoms of choline groups, phosphate atoms, and carbonyl oxygens are presented for lipid molecules. For the system with full hydration (POPC-CEL-30H₂O), we observe the component-wise lipid density profiles typical for free-standing bilayers. Decreasing the hydration level of the interfacial region from 30 to 20 water molecules per lipid leads to the appearance of a small peak in the distribution of choline lipid groups; see Figure 5. This is a signature that a lipid bilayer starts to interact with the cellulose surface; see also Table 2. These effects become much more pronounced when hydration of a lipid bilayer further drops. In the POPC-CEL-10H₂O system, the peaks of the profiles of choline and phosphate groups become narrower and higher, shifting toward the support surface. Furthermore, an additional peak in the density distribution of phosphate groups appears, indicating the attraction of the lipid phosphates to the cellulose surface. In the case of the “dry” interfacial region (POPC-CEL-0H₂O), one can even observe an overlap of the profiles of cellulose and lipid atoms (Figure 5). It is also seen that the lipid phosphate groups increase significantly their presence at the cellulose surface. We note that hydroxyl groups are shorter than exocyclic hydroxymethyl groups, so that the corresponding peaks of atoms O6(O16) are closer to the bilayer. Therefore, one can expect stronger interactions of lipid head groups with atoms O6(O16) as compared to atoms O2(O12) and O3(O13).

The presence of a support in the vicinity of a bilayer leaflet induces changes in the structural organization of the water phase. The orientation of water molecules in a bilayer system can be characterized by the angle between the water dipoles and the outward bilayer normal.³² In Figure 6, we present the average cosine of this angle as a function of the distance from the center of a bilayer. Bulk water corresponds to the regions in Figure 6 in which $\langle \cos \theta \rangle$ equals zero, which implies that there is no preferential orientation of water molecules. Such regions can be observed for water baths at the distal bilayer leaflets in all systems under study. As far as the interfacial bilayer–cellulose regions are concerned, strictly speaking, we do not observe bulk water there even for the system with full hydration (POPC-CEL-30H₂O). Closer to the lipid/water interface $\langle \cos \theta \rangle$ has negative values, which is a sign that hydrogen atoms of water molecules are directed toward the membrane. In turn, close to the cellulose crystalline surface one has relatively large oscillations of $\langle \cos \theta \rangle$ due to strong interactions of cellulose’s hydroxyl and hydroxymethyl groups with water molecules. These two interfacial (lipid–water and cellulose–water) regions get closer to each other upon decreasing the average bilayer–cellulose distance and overlap when hydration level becomes 10 H₂O molecules per lipid; see Figure 6.

Lipid Head Group Orientation and Ordering of Lipid Acyl Chains. To characterize the support-induced changes in the structural properties of phospholipid bilayers, we probed the orientation of lipid head groups and the order parameter of

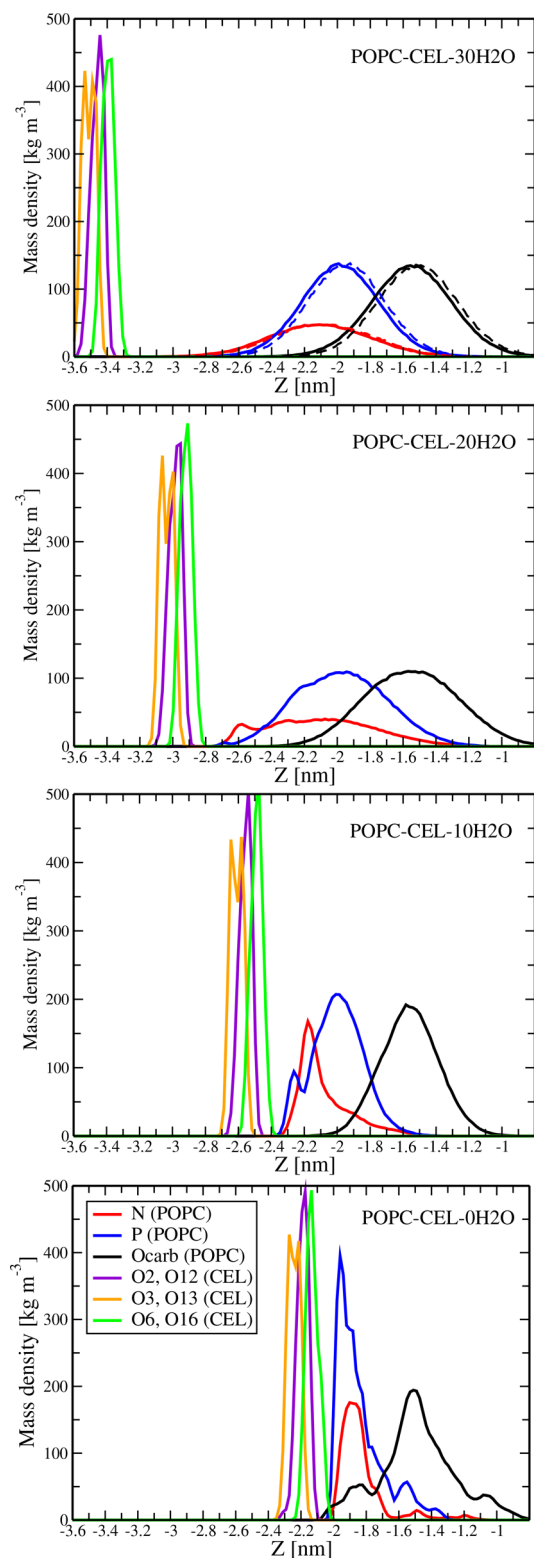


Figure 5. Component-wise mass density profiles for principal atoms of lipid molecules and cellulose chains as a function of the distance from the bilayer center ($Z = 0$). Shown are the profiles for nitrogen, phosphorus, and carbonyl oxygen atoms of POPC lipid molecules and for oxygen atoms of hydroxyl and hydroxymethyl groups of a cellulose support. The profiles for a free-standing bilayer are shown by dashed lines (top plot).

lipid hydrocarbon tails. For a free-standing POPC lipid bilayer, the average angle between PN (phosphorus–nitrogen) vectors

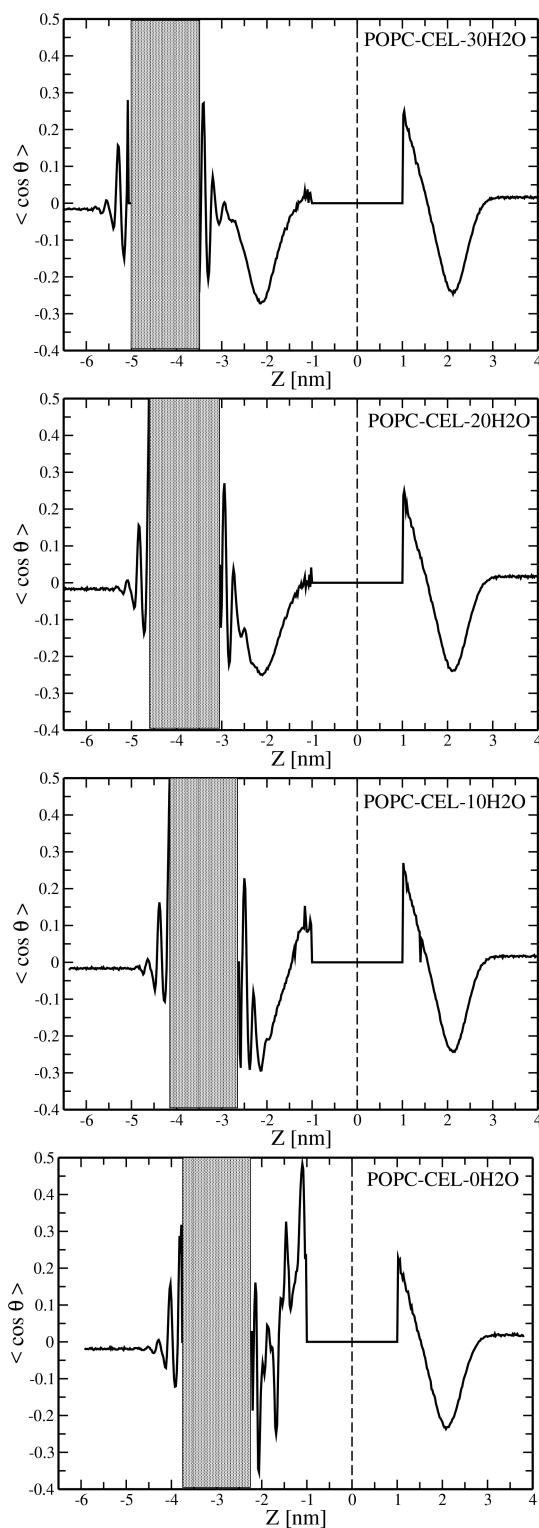


Figure 6. Average cosine of the angle between water dipoles and the outward bilayer normal as a function of the distance from the bilayer center ($Z = 0$) for all considered cellulose–bilayer systems. The location of a cellulose crystal is shown in gray, and the center of mass of a lipid bilayer is denoted by a vertical dashed line.

of phospholipid head groups and the outward bilayer normal was found to be $69.5^\circ \pm 0.1^\circ$ in line with previous simulation data.³³ For the angle of the PN vector of distal leaflets of all four lipid–cellulose systems and proximal leaflets of systems POPC-CEL-30H2O and POPC-CEL-20H2O, we found very

close values: $68.5^\circ \pm 0.1^\circ$ and $70.7^\circ \pm 0.1^\circ$, respectively. To visualize the robustness of the lipid head group orientation at a relatively large level of hydration, in Figure 7, we plot the

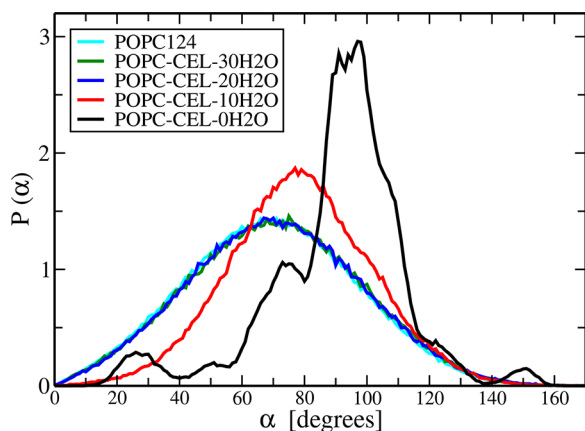


Figure 7. Probability distribution function of the angle between PN vectors of phospholipids and the outward bilayer normal for the bilayer leaflets next to the surface of a cellulose crystal.

probability distribution function for the angle in question. Indeed, the angle distributions for a free-standing bilayer and supported bilayers with 30 and 20 water molecules per lipid of the proximal leaflet practically coincide.^{7,9} The situation changes drastically when the hydration level of the interfacial lipid–cellulose region drops below 20 H₂O: the distribution peaks become pronouncedly higher and shift toward larger values of the PN angle, implying a considerable (more horizontal) reorientation of lipid head groups due to the interactions of lipids with cellulose chains, see Figure 7. Indeed, one has the average PN vector angle of $78.6^\circ \pm 0.1^\circ$ for the proximal leaflet of the system POPC-CEL-10H₂O (and even $90.5^\circ \pm 0.1^\circ$ for the “dry” lipid–cellulose system, i.e., in this case the lipids head groups on average lie parallel to the surface of the bilayer).

Another important structural characteristic of a lipid bilayer is related to the ordering of lipid acyl chains. To this end, we calculated the deuterium order parameters of sn-1 (saturated) lipid chains for all lipid–cellulose systems under study; see Figure 8. It turns out that the ordering of acyl lipid tails is insensitive to the presence of a cellulose-based support as long as lipid head groups are hydrated with water (systems POPC-CEL-30H₂O, POPC-CEL-20H₂O, and POPC-CEL-10H₂O). In contrast, for the “dry” system (POPC-CEL-0H₂O) we observed a pronounced drop in the order parameter.

The hydrophobic lipid chains do not interact with a cellulose support directly; the only impact of the support is in dehydration of the lipid bilayer. Such a dehydration in free-standing tensionless lipid bilayers leads to the decrease of the area per lipid and correspondingly to the enhanced ordering of lipid acyl chains.^{34–36} As the area per lipid is fixed in our systems, we do not see this chain ordering when the hydration drops from 30 to 10 water molecules per lipid. This is obviously a limitation of the approach used here. Furthermore, the disordering seen for the “dry” system can also be considered as an artifact of the fixed-area simulations: a complete removal of water molecules from the lipid–water interface leads to an increase in the free volume available for lipids under fixed-area conditions.

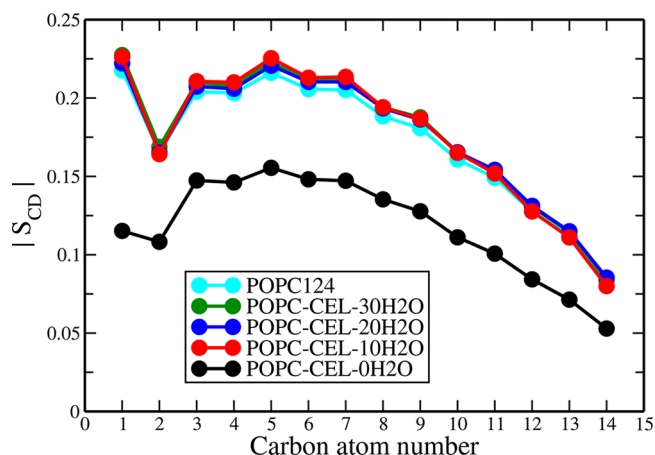


Figure 8. Deuterium order parameters $|S_{CD}|$ of sn-1 (saturated) lipid chains of the proximal leaflets for all bilayer–cellulose systems considered.

Lipid–Cellulose Interactions. To get insight into the molecular details of the interactions of lipid molecules with a cellulose crystal, we calculated radial distribution functions (RDF) for various pairs of lipid and cellulose atoms and identified the pairs for which RDFs were characterized by a well-defined peak, thereby implying the existence of strong interactions between these two atoms. It turns out that the lipid–cellulose interactions are mainly governed by the interactions between polar lipid head groups (choline and phosphate groups) and cellulose’s hydroxyl and hydroxymethyl groups. The rest of lipid–cellulose contacts play only a rudimentary role.

In Figure 9, we show radial distribution functions for lipid choline groups (or nitrogen atoms) and principal oxygen atoms of cellulose chains: O2(O12), O3(O13), and O6(O16); see Figure 2 for the atom definition. One can see that the height of the RDF peaks increases systematically when the bilayer–support distance (interfacial hydration) goes down. In the case of full hydration of the interfacial region (system POPC-CEL-30H₂O), the RDFs do not develop any peaks, which is a sign of the absence of contacts and correspondingly lipid–cellulose interactions.

Based on the RDFs we calculated the average number of contacts between lipid choline groups (nitrogen atoms) and cellulose oxygen atoms. The calculations were carried out in line with ref 37 by counting the number of oxygen atoms within the first coordination spheres of nitrogen atoms; the radii of the first coordination spheres were identified from the positions of first minima of the RDFs; see Figure 9. The resulting numbers of contacts per POPC lipid are listed in Table 3. First of all, it is clearly seen that the largest number of cellulose–choline contacts is observed for exocyclic hydroxymethyl groups (groups of carbon C6(C16)) most likely due to a larger length of the hydroxymethyl groups. As for shorter hydroxyl groups, the number of contacts for atoms O2(O12) turns out to be considerably larger than that for atoms O3(O13). A possible underlying reason consists in the fact that atoms O3(O13) are somewhat more hidden within the cellulose surface (see Figure 2) and therefore less accessible for choline groups of lipids. Furthermore, decreasing the distance between a bilayer and a cellulose support leads to a systematic increase of all the numbers of contacts considered; see Table 3. In line with what was mentioned above for the system POPC-CEL-30H₂O, the

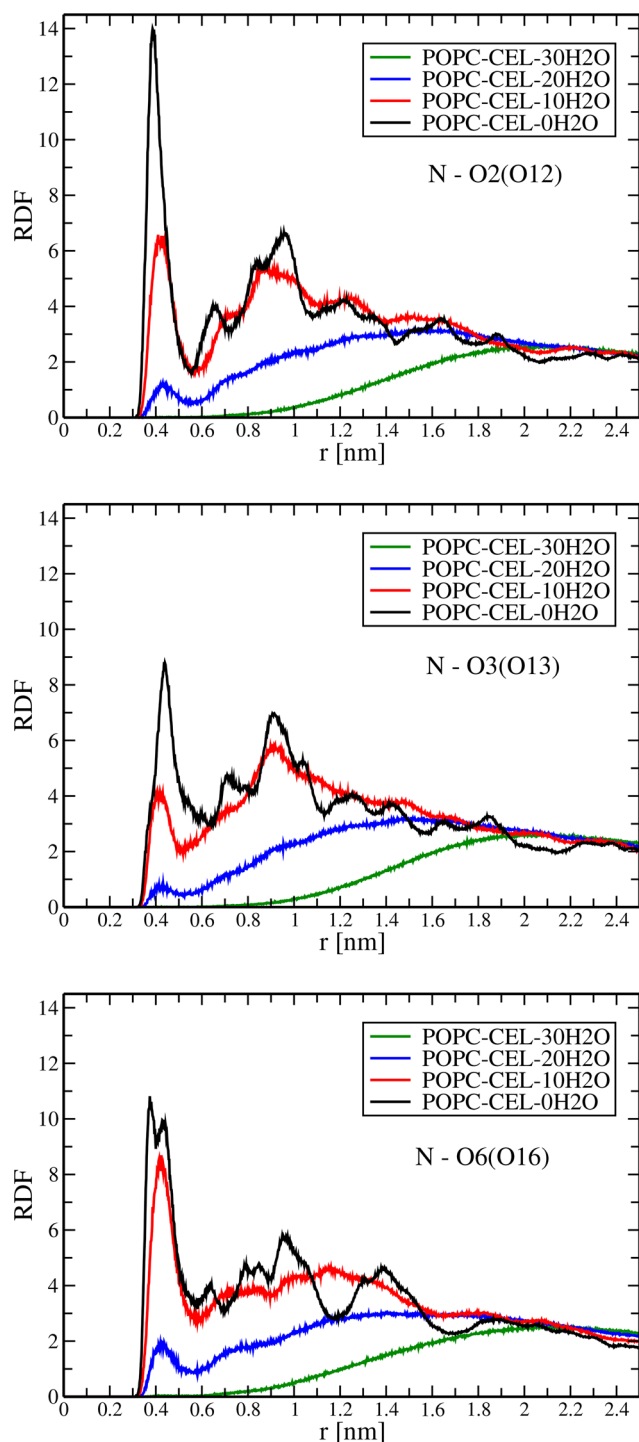


Figure 9. Radial distribution functions (RDFs) of nitrogen atoms of lipid head groups and oxygen atoms of hydroxyl (O2(O12) and O3(O13)) and hydroxymethyl (O6(O16)) groups of a cellulose crystal.

corresponding numbers of cellulose-lipid contacts at full hydration of the interfacial region are indeed vanishing.

Another very important mode of interactions between lipid molecules and the cellulose surface is hydrogen bonding between phosphate groups of lipids and hydroxyl (hydroxymethyl) groups of cellulose. Phosphate groups are located considerably deeper inside a lipid bilayer as compared to choline groups, so that one has to have a rather close juxtaposition between a bilayer and a support to establish this type of interactions. Therefore, for the cellulose-bilayer systems with the interfacial water the peaks of RDFs for lipid phosphate groups and cellulose's oxygen atoms are clearly seen only for the system with low hydration (POPC-CEL-10H2O) and mainly for hydroxymethyl groups O6(O16); see Figure 10. Similar to many other characteristics, the “dry” POPC-CEL-0H2O system shows much more pronounced peaks for RDFs. In Table 4, we summarize the number of hydrogen bonds between lipid phosphate groups and hydroxyl (hydroxymethyl) groups of cellulose. For the calculation of hydrogen bonds, the following geometrical criteria were used: the donor–acceptor distance was smaller than 0.35 nm and the hydrogen–donor–acceptor angle was smaller than 30°. For systems POPC-CEL-10H2O and POPC-CEL-20H2O, the largest number of hydrogen bonds with a lipid bilayer is formed by hydroxymethyl groups of cellulose. For the limiting case of the “dry” cellulose–lipid system (POPC-CEL-0H2O), hydroxyl groups O2(O12) also become very important: the corresponding number of hydrogen bonds turns out to be rather close to that observed for hydroxymethyl groups O6(O16); see Table 4.

The above two types of lipid–cellulose interactions are largely responsible for the changes that a cellulose nanocrystal support induces on a phospholipid bilayer. When the hydration level of the interfacial bilayer/support region is low, these interactions give rise to a pronounced asymmetry in the properties of the opposite bilayer leaflets. In particular, hydrogen bonding between lipid phosphate groups and hydroxymethyl/hydroxyl groups of cellulose pulls some of the phosphates toward the water/lipid interface. This leads to the observed splitting of the density profile of the proximal bilayer leaflets into two peaks (Figure 4) as well as more horizontal reorientation of lipid head groups with respect to the bilayer surface (Figure 7). In addition to the changes in the structure of the proximal leaflets, one can anticipate that the hydrogen bonding between lipids and cellulose should also slow down the lateral mobility of lipids in these leaflets. This is indeed seen through inspection of the mean-square displacements³⁸ of lipid molecules which is presented in Figure 11. A pronounced decrease in the lateral mobility of lipids is observed in the proximal leaflets of the system POPC-CEL-10H2O (and also POPC-CEL-0H2O), i.e., in the systems that are characterized by the strongest lipid–cellulose hydrogen bonding; see Table 4. Note that the lateral lipid mobility measured in atomic-scale MD simulations is often characterized by a considerable uncertainty (see the error bars shown for one of the systems

Table 3. Number of Contacts of Lipid Choline Groups (Nitrogen Atoms) With Oxygen Atoms of Cellulose (per POPC Lipid)

	N–O2(O12)	N–O3(O13)	N–O6(O16)
POPC-CEL-30H2O	0.0020 ± 0.0002	0	0.0047 ± 0.0004
POPC-CEL-20H2O	0.150 ± 0.004	0.062 ± 0.002	0.242 ± 0.005
POPC-CEL-10H2O	0.762 ± 0.005	0.355 ± 0.004	1.040 ± 0.007
POPC-CEL-0H2O	1.177 ± 0.003	0.749 ± 0.002	1.455 ± 0.005

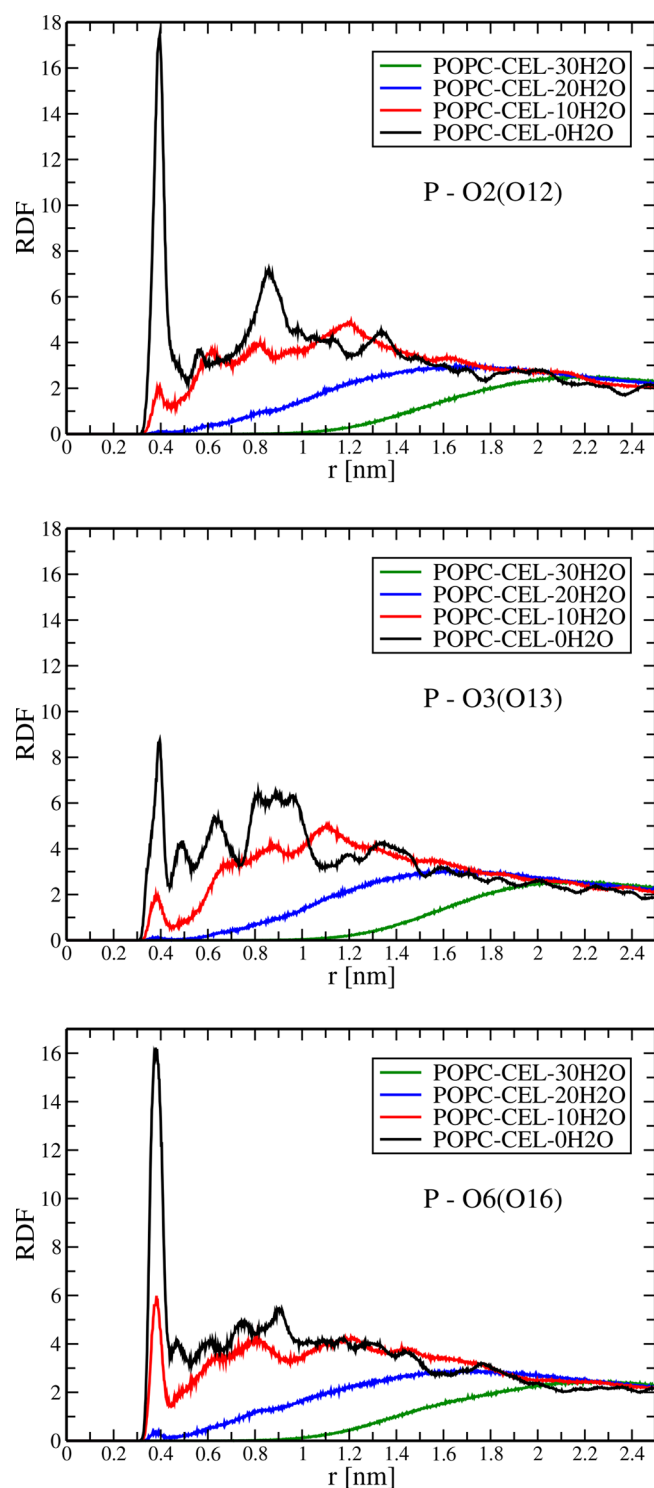


Figure 10. Radial distribution functions (RDFs) of phosphorus atoms of lipid head groups and oxygen atoms of hydroxyl (O2(O12) and O3(O13)) and hydroxymethyl (O6(O16)) groups of a cellulose crystal.

in Figure 11), which explains the observed scattering of data for the MSDs of lipids in distal bilayer leaflets of the systems considered.

DISCUSSION AND CONCLUSIONS

Interactions of cellulose nanocrystals with phospholipids represent an important problem from the point of view of

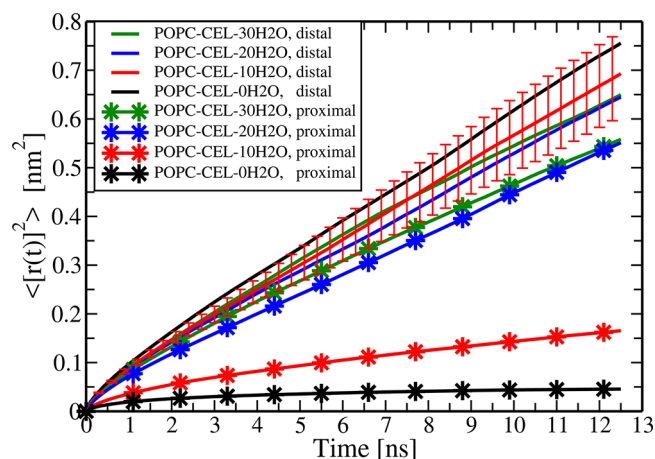
cellulose-based dressing materials and their impact on living tissues (wounds). Despite their importance, the molecular mechanisms behind such interactions have not been unlocked yet. Our computational study aims to meet lack of the detailed molecular-level information regarding the interfacial region between the cellulose-based dressing and cell membranes. To this end, we performed a series of atomistic computer simulations of phospholipid bilayers on a crystalline cellulose support at various hydration levels of the bilayer leaflets next to the cellulose surface. Our findings clearly show for the first time the existence of strong interactions between polar lipid head groups and the hydrophilic surface of a cellulose crystal. The strength of these interactions increases with a decrease of the bilayer-cellulose distance (or with a drop in the hydration level of the interfacial lipid/cellulose region). We identified two major types of interactions between phospholipid molecules and cellulose chains: (i) direct attractive interactions between lipid choline groups and oxygens of hydroxyl (hydroxymethyl) groups of cellulose and (ii) hydrogen bonds between phosphate groups of lipids and cellulose's hydroxymethyl/hydroxyl groups. Both these types of lipid–cellulose interactions are largely responsible for the changes that a cellulose nanocrystal support induces on a phospholipid bilayer. When the hydration level of the interfacial bilayer/support region is low, these interactions give rise to a pronounced asymmetry in the properties of the opposite bilayer leaflets. In particular, we witness splitting of the density profile of the proximal leaflets into two peaks as well as more horizontal reorientation of lipid head groups with respect to the bilayer surface. Both these effects are likely due to hydrogen bonding between lipid phosphate groups and hydroxymethyl/hydroxyl groups of cellulose, which pulls phosphates toward the water–lipid interface. Furthermore, the hydrogen bonding is found to considerably slow down the lateral mobility of lipids in the leaflets next to the cellulose surface at low hydration of the lipid–cellulose interfacial region.

As molecular-level insight into the interactions between lipid bilayers and crystalline cellulose is beyond the resolution of most experimental techniques, it can be useful for identifying possible strategies for improving the properties of cellulose-based dressing materials. In particular, our results clearly demonstrate that the exocyclic hydroxymethyl groups O6(O16) of cellulose have much better access to both choline and phosphate groups of phospholipids as compared to hydroxyl groups. Furthermore, at a very close juxtaposition between a lipid bilayer and a cellulose crystal the contribution of the hydroxyl groups O2(O12) into the lipid/cellulose interactions becomes comparable with that of hydroxymethyl groups O6(O16). Therefore, the groups of these two types can be considered as primary targets for chemical modification of the surface of cellulose nanocrystals with the aim to modify the adhesion of a cellulose-based dressing material to the living tissues. In particular, a chemical modification that inhibits the ability of the hydroxymethyl/hydroxyl groups of cellulose to form hydrogen bonds with lipids could weaken considerably the undesirable adhesive interactions between cellulose-based materials and cell membranes.

The primary focus of our study was on the interactions of cellulose-based materials with biological membranes. As a first step, we studied here lipid bilayers built from phosphatidylcholine lipids; such model bilayer systems are often used to probe the basic structural properties of cell membranes. However, the lipid composition of cell membranes is much more complex; in

Table 4. Number of Hydrogen Bonds between Hydroxyl (Hydroxymethyl) Groups of Cellulose and Oxygen Atoms of Phosphate Groups of Lipids (per POPC Lipid)

	O2(O12)	O3(O13)	O6(O16)
POPC-CEL-30H2O	0	0	0
POPC-CEL-20H2O	0.0027 ± 0.0006	0.0027 ± 0.0005	0.011 ± 0.001
POPC-CEL-10H2O	0.060 ± 0.003	0.051 ± 0.002	0.186 ± 0.004
POPC-CEL-0H2O	0.632 ± 0.003	0.306 ± 0.001	0.640 ± 0.004

**Figure 11.** Lateral mean-square displacements of POPC lipids for all bilayer–cellulose systems considered. Shown are the results for both distal (lines without symbols) and proximal (lines with stars) bilayer leaflets. Error bars (the standard deviation) are shown for the distal leaflet of the POPC-CEL-10H2O system.

addition to phosphatidylcholines, the membranes also contain other types of lipids such as sphingomyelin, phosphatidylethanolamine, and phosphatidylserine lipids.³⁹ Head groups of most of these lipids are capable to intermolecular hydrogen-bonding that could enhance further the attractive interactions of a cellulose crystal with the membrane surface. The same also might apply to ceramide lipids that constitute a major component of the topmost layer of the skin.

Another interesting problem that cannot be handled with the methodology used in this study is related to the determination of the equilibrium hydration level of the interfacial region between a cellulose support and a lipid bilayer. Given the fact that the system with hydration level of 10 water molecules per lipid is well equilibrated and the “dry” system demonstrates net water flux toward the interfacial region, one can expect that the equilibrium hydration level would intermediate between these two values. To calculate the equilibrium hydration level, one needs to provide an access of bulk water to the interfacial bilayer-support region. This can be achieved, e.g., through the creation of an artificial pore in the support (similar to ref 7) and by performing the umbrella sampling calculations. This is a subject of our ongoing studies.

■ ASSOCIATED CONTENT

Supporting Information

The Supporting Information is available free of charge on the ACS Publications website at DOI: 10.1021/acs.langmuir.7b02297.

Plots for bilayer-cellulose distances as a function of time; snapshots of diffusion of a water molecules across a lipid bilayer; additional results for a cellulose-bilayer system of an increased size (PDF)

■ AUTHOR INFORMATION

Corresponding Author

*E-mail: a.gurtovenko@gmail.com. Web: biosimu.org. Phone: +7-812-3285601. Fax: +7-812-3286869.

ORCID

Andrey A. Gurtovenko: 0000-0002-9834-1617

Notes

The authors declare no competing financial interest.

■ ACKNOWLEDGMENTS

The authors wish to acknowledge the use of the computer cluster of the Institute of Macromolecular Compounds RAS and the Lomonosov supercomputer at the Moscow State University. This work was supported by the Russian Ministry of Education and Science within State Contract 14.W03.31.0014 (megagrant).

■ REFERENCES

- Doelker, E. Cellulose derivatives. *Adv. Polym. Sci.* **1993**, *107*, 199–265.
- Qiu, X.; Hu, S. “Smart” Materials Based on Cellulose: A Review of the Preparations, Properties, and Applications. *Materials* **2013**, *6*, 738–781.
- Boateng, J. S.; Matthews, K. H.; Stevens, H. N. E.; Eccleston, G. M. Wound healing dressings and drug delivery systems: A review. *J. Pharm. Sci.* **2008**, *97*, 2892–2923.
- Ristic, T.; Zemljic, L. F.; Novak, M.; Kuncic, M. K.; Sonjak, S.; Cimerman, N. G.; Strnad, S. In *Science against microbial pathogens: communicating current research and technological advances*; Mendez-Vilas, A., Ed.; Formatex Research Center: Badajoz, Spain, 2011; pp 36–51.
- Yamanaka, S.; Watanabe, K.; Kitamura, N.; Iguchi, M.; Mitsuhashi, S.; Nishi, Y.; Uryu, M. The structure and mechanical properties of sheets prepared from bacterial cellulose. *J. Mater. Sci.* **1989**, *24*, 3141–3145.
- Bshena, O.; Heunis, T. D. J.; Dicks, L. M. T.; Klumperman, B. Antimicrobial fibers: therapeutic possibilities and recent advances. *Future Med. Chem.* **2011**, *3*, 1821–1847.
- Roark, M.; Feller, S. E. Structure and Dynamics of a Fluid Phase Bilayer on a Solid Support as Observed by a Molecular Dynamics Computer Simulation. *Langmuir* **2008**, *24*, 12469–12473.
- Hartshorn, C. M.; Jewett, C. M.; Brozik, J. A. Molecular Effects of a Nanocrystalline Quartz Support upon Planar Lipid Bilayers. *Langmuir* **2010**, *26*, 2609–2617.
- Varma, S.; Teng, M.; Scott, H. L. Nonintercalating Nano-substrates Create Asymmetry between Bilayer Leaflets. *Langmuir* **2012**, *28*, 2842–2848.
- Duro, N.; Gjika, M.; Siddiqui, A.; Scott, H. L.; Varma, S. POPC Bilayers Supported on Nanoporous Substrates: Specific Effects of Silica-Type Surface Hydroxylation and Charge Density. *Langmuir* **2016**, *32*, 6766–6774.
- Xing, C. Y.; Faller, R. Interactions of lipid bilayers with supports: A coarse-grained molecular simulation study. *J. Phys. Chem. B* **2008**, *112*, 7086–7094.
- Xing, C. Y.; Faller, R. Coarse-grained simulations of supported and unsupported lipid monolayers. *Soft Matter* **2009**, *5*, 4526–4530.

- (13) Xing, C. Y.; Ollila, O. H. S.; Vattulainen, I.; Faller, R. Asymmetric nature of lateral pressure profiles in supported lipid membranes and its implications for membrane protein functions. *Soft Matter* **2009**, *5*, 3258–3261.
- (14) Lamberg, A.; Taniguchi, T. Coarse-Grained Computational Studies of Supported Bilayers: Current Problems and Their Root Causes. *J. Phys. Chem. B* **2014**, *118*, 10643–10652.
- (15) Tolmachev, D. A.; Lukasheva, N. V. Interactions Binding Mineral and Organic Phases in Nanocomposites Based on Bacterial Cellulose and Calcium Phosphates. *Langmuir* **2012**, *28*, 13473–13484.
- (16) Lukasheva, N. V.; Tolmachev, D. A. Cellulose Nanofibrils and Mechanism of their Mineralization in Biomimetic Synthesis of Hydroxyapatite/Native Bacterial Cellulose Nanocomposites: Molecular Dynamics Simulations. *Langmuir* **2016**, *32*, 125–134.
- (17) Nishiyama, Y.; Langan, P.; Chanzy, H. Crystal Structure and Hydrogen-Bonding System in Cellulose I β from Synchrotron X-ray and Neutron Fiber Diffraction. *J. Am. Chem. Soc.* **2002**, *124*, 9074–9082.
- (18) Kucerka, N.; Tristram-Nagle, S.; Nagle, J. F. Structure of fully hydrated fluid phase lipid bilayers with monounsaturated chains. *J. Membr. Biol.* **2006**, *208*, 193–202.
- (19) Klauda, J. B.; Venable, R. M.; Freites, J. A.; O'Connor, J. W.; Tobias, D. J.; Mondragon-Ramirez, C.; Vorobyov, I.; MacKerell, A. D.; Pastor, R. W. Update of the CHARMM All-Atom Additive Force Field for Lipids: Validation on Six Lipid Types. *J. Phys. Chem. B* **2010**, *114*, 7830–7843.
- (20) Guvench, O.; Greene, S. N.; Kamath, G.; Brady, J. W.; Venable, R. M.; Pastor, R. W.; Mackerell, A. D. Additive Empirical Force Field for Hexopyranose Monosaccharides. *J. Comput. Chem.* **2008**, *29*, 2543–2564.
- (21) Guvench, O.; Hatcher, E.; Venable, R. M.; Pastor, R. W.; MacKerell, A. D. CHARMM Additive All-Atom Force Field for Glycosidic Linkages between Hexopyranoses. *J. Chem. Theory Comput.* **2009**, *5*, 2353–2370.
- (22) Paavilainen, S.; Rog, T.; Vattulainen, I. Analysis of twisting of cellulose nanofibrils in atomistic molecular dynamics simulations. *J. Phys. Chem. B* **2011**, *115*, 3747–3755.
- (23) Hadden, J. A.; French, A. D.; Woods, R. J. Unraveling Cellulose Microfibrils: A Twisted Tale. *Biopolymers* **2013**, *99*, 746–756.
- (24) MacKerell, A. D.; et al. All-Atom Empirical Potential for Molecular Modeling and Dynamics Studies of Proteins. *J. Phys. Chem. B* **1998**, *102*, 3586–3616.
- (25) Berendsen, H. J. C.; Postma, J. P. M.; van Gunsteren, W. F.; DiNola, A.; Haak, J. R. Molecular dynamics with coupling to an external bath. *J. Chem. Phys.* **1984**, *81*, 3684–3690.
- (26) Nosé, S. A molecular dynamics method for simulations in the canonical ensemble. *Mol. Phys.* **1984**, *52*, 255–268.
- (27) Hoover, W. G. Canonical dynamics: equilibrium phase-space distributions. *Phys. Rev. A: At., Mol., Opt. Phys.* **1985**, *31*, 1695–1697.
- (28) Parrinello, M.; Rahman, A. Polymorphic transitions in single crystals: A new molecular dynamics method. *J. Appl. Phys.* **1981**, *52*, 7182–7190.
- (29) Hess, B.; Bekker, H.; Berendsen, H. J. C.; Fraaije, J. G. E. M. LINCS: A linear constraint solver for molecular simulations. *J. Comput. Chem.* **1997**, *18*, 1463–1472.
- (30) Essmann, U.; Perera, L.; Berkowitz, M. L.; Darden, T.; Lee, H.; Pedersen, L. G. A smooth particle mesh Ewald method. *J. Chem. Phys.* **1995**, *103*, 8577–8593.
- (31) Abraham, M. J.; Murtola, T.; Schulz, R.; Pall, S.; Smith, J.; Hess, B.; Lindahl, E. Gromacs: High Performance Molecular Simulations through Multi-Level Parallelism from Laptops to Supercomputers. *SoftwareX* **2015**, *1-2*, 19–25.
- (32) Kostitskii, A. Y.; Kondinskaia, D. A.; Nesterenko, A. M.; Gurtovenko, A. A. Adsorption of Synthetic Cationic Polymers on Model Phospholipid Membranes: Insight from Atomic-Scale Molecular Dynamics Simulations. *Langmuir* **2016**, *32*, 10402–10414.
- (33) Antipina, A. Y.; Gurtovenko, A. A. Molecular mechanism of calcium-induced adsorption of DNA on zwitterionic phospholipid membranes. *J. Phys. Chem. B* **2015**, *119*, 6638–6645.
- (34) Mashl, R. J.; Scott, H. L.; Subramaniam, S.; Jakobsson, E. Molecular Simulation of Dioleoylphosphatidylcholine Lipid Bilayers at Differing Levels of Hydration. *Biophys. J.* **2001**, *81*, 3005–3015.
- (35) Hogberg, C. J.; Lyubartsev, A. P. A Molecular Dynamics Investigation of the Influence of Hydration and Temperature on Structural and Dynamical Properties of a Dimyristoylphosphatidylcholine Bilayer. *J. Phys. Chem. B* **2006**, *110*, 14326–14336.
- (36) Dvinskikh, S. V.; Castro, V.; Sandstrom, D. Probing segmental order in lipid bilayers at variable hydration levels by amplitude- and phase-modulated cross-polarization NMR. *Phys. Chem. Chem. Phys.* **2005**, *7*, 3255–3257.
- (37) Gurtovenko, A. A.; Vattulainen, I. Effect of NaCl and KCl on phosphatidylcholine and phosphatidylethanolamine lipid membranes: Insight from atomic-scale simulations for understanding salt-induced effects in the plasma membrane. *J. Phys. Chem. B* **2008**, *112*, 1953–1962.
- (38) Miettinen, M. S.; Gurtovenko, A. A.; Vattulainen, I.; Karttunen, M. Ion Dynamics in Cationic Lipid Bilayer Systems in Saline Solutions. *J. Phys. Chem. B* **2009**, *113*, 9226–9234.
- (39) Gennis, R. B. *Biomembranes: Molecular Structure and Function*; Springer-Verlag: New York, 1989.